Progress In Electromagnetics Research M, Vol. 52, 141–152, 2016

Analysis of Scattering from Composite Conductor and Dielectric Objects Using Single Integral Equation Method and MLFMA Based on JMCFIE

Hua-Long Sun*, Chuang-Ming Tong, and Peng Peng

Abstract—A highly efficient hybrid method of single integral equation (SIE) and electric/magnetic current combined field integral equation (JMCFIE) is presented, named as SJMCFIE, for analysing scattering from composite conductor and dielectric objects, in which, SIE can reduce one half unknowns in dielectric region. The resultant matrix equation of SJMCFIE can be represented in the iteration form, which makes the computation complexity reduced further, and coupling mechanism of composite model becomes more explicit. For accelerating matrix-vector multiplications (MVMs), Multilevel Fast Multipole Algorithm (MLFMA) is employed to combine SJMCFIE to formulate SJMCFIE-MLFMA at last, which is the extension of SIE-MLFMA in the proposed reference. Finally, some examples verify the new hybrid method on accuracy, memory storage, computation efficiency compared to SIE-MLFMA and JMCFIE-MLFMA. Besides, SJMCFIE-MLFMA can also be used to analyse the complete coated model's scattering.

1. INTRODUCTION

Analyzing electromagnetic scattering from composite conductor and dielectric objects has gained wide interest from many researchers, which have the importance in studying coated targets, cavity filled with dielectric materials, printed antenna on substrate, and substrate integrated waveguide (SIW). Specially, the research on stealthy weapon platforms and system, and the target's recognition motivates the requirement for precisely computing and analyzing the target's electromagnetic scattering. Traditional high-frequency asymptotic methods are not suitable for this kind of requirement due to poor accuracy in spatial, angular and frequency domain, whereas numerical algorithms are suitable for this situation due to their high precision. Computing composite models can utilize the methods based on surface integral equation [1–4], hybrid volume-surface integral equations [5], or Finite-Element-Boundary-integral techniques [6]. The methods based on surface integral equation have the advantage over hybrid volume-surface integral equation on computing homogeneous material objects. In practice, when analyzing scattering from composite objects based on surface integral equations, the conducting part usually utilizes electric field integral equation (EFIE), magnetic field integral equation or combined field integral equation, and the dielectric part utilizes Poggio-Miller-Chang-Harrington-Wu-Tsai (PMCHWT) equations [7], electric and magnetic current combine field integral equation (JMCFIE) [8–12], or N-Müller integral equations [13]. Especially, formulating equations in the dielectric part concerns both equivalent electric and magnetic currents. Yeung [14] proposes single integral equation (SIE), which only concerns the effective currents rather than both electric and magnetic currents, and as a result, the unknowns of SIE are only one half of JMCFIE or PMCHWT. However, SIE in [14] is only used to analyze the pure dielectric objects. Then, Wang et al. [15] extend SIE to analyze the combined conducting and

Received 13 August 2016, Accepted 12 November 2016, Scheduled 6 December 2016
* Corresponding author: Hua-Long Sun (hualongsun1982@163.com).
The authors are with the Air and Missile Defense College, Air Force Engineering University, Xi'an 710051, China.

dielectric bodies, and incorporate multilevel fast multipole algorithm (MLFMA) [16, 17] as the extension of fast multipole method (FMM) [18] to reduce the complexity of matrix-vector products. It is worth to note that SIE-MLFMA in [15] is based on EFIE, so its iteration convergence is usually slower than that of magnetic field integral equation and magnetic field integral equation.

In this paper, a highly efficient hybrid method of SIE and JMCFIE is presented, named as SJMCFIE, to perform scattering from composite conductor and dielectric objects, which has two advantages: one is that JMCFIE guarantees fast convergence of iteratively solving compared to EFIE in SIE-MLFMA [15], and the other is that further SIE translates non-compact operators into compact operators [19–21] to achieve fast convergence of iteratively solving compared to JMCFIE. SJMCFIE can be rewritten in new iteration form, which not only reduces computation complexity, but also makes coupling mechanism explicit. With the unknowns of composite conductor and dielectric objects, solving resultant matrix equation based SJMCFIE gets harder. Like SIE-MLFMA, SJMCFIE-MLFMA is obtained by adopting MLFMA to accelerate MVMs. Examples show that: SJMCFIE-MLFMA has higher efficiency and accuracy than SIE-MLFMA and JMCFIE-MLFMA. Finally, SJMCFIE-MLFMA can also be used to analyze scattering from the complete coated model.

2. FORMULATION

2.1. Hybrid Method of SIE and JMCFIE

A typical model of composite conductor and dielectric objects is shown in Fig. 1. S_1 and S_2 are the surfaces of the conductor and dielectric domain, respectively. S_3 is the common interface of the conductor and dielectric domain. $\mathbf{J}_{1e}$ is induced electric current on the exterior surface S_1, and $\mathbf{J}_{2e}$ and $\mathbf{J}_{2m}$ are equivalent surface electric and magnetic currents on the exterior surface of S_2. J_{2e}^{eff} is single effective current on the interior surface of the dielectric domain enclosed by S_2 and S_3. ε_0 and μ_0 are the permittivity and permeability in the free space, respectively. ε and μ are the permittivity and permeability in the dielectric region, respectively.

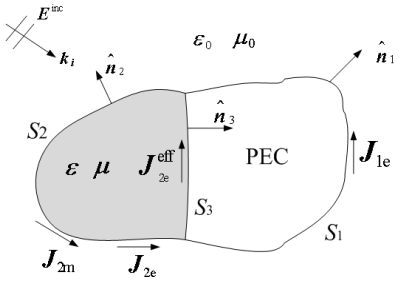

Figure 1. Illustration of composite conductor and dielectric objects illuminated by the incident.

Scattering field outside S_1 and S_2 can be computed by $\mathbf{J}_{1e}$ located on the exterior surface S_1, and $\mathbf{J}_{2e}$ and $\mathbf{J}_{2m}$ located on the exterior surface S_2:

$$\mathbf{E}^s = \eta_0 L_0(\mathbf{J}_{1e}) + \eta_0 L_0(\mathbf{J}_{2e}) - K_0(\mathbf{J}_{2m}) \quad H^s = K_0(\mathbf{J}_{1e}) + (1/\eta_0) L_0(\mathbf{J}_{2m}) + K_0(\mathbf{J}_{2e}) \tag{1}$$

where subscript 0 denotes the free space, and $L_0(\cdot)$ and $K_0(\cdot)$ are electric field integral operator and magnetic field integral operator, respectively:

$$L_0(\mathbf{f}) = -jk_0 \int_{S_m} [g_0(\mathbf{r}, \mathbf{r}')\mathbf{f}(\mathbf{r}') + (1/k_0^2)\nabla g_0(\mathbf{r}, \mathbf{r}')\nabla' \cdot \mathbf{f}(\mathbf{r}')]dS' \quad m = 1, 2 \tag{2a}$$

$$K_0(\mathbf{f}) = -\int_{S_m} [\mathbf{f}(\mathbf{r}') \times \nabla g_0(\mathbf{r}, \mathbf{r}')]dS' \quad m = 1, 2 \tag{2b}$$

with $g_0(\mathbf{r}, \mathbf{r}') = \exp(-jk_0|\mathbf{r} - \mathbf{r}'|)/(4\pi|\mathbf{r} - \mathbf{r}'|)$ being the Green's function in the free space and $\eta_0 = \sqrt{\mu_0/\varepsilon_0}$ the wave impedance in the free space. Total electric and magnetic fields satisfy the

boundary condition of the JMCFIE formulation [4, 11]:

$$\begin{cases} \mathbf{e}_1(\mathbf{r}) = \mathbf{e}_1^{inc}(\mathbf{r}) + \mathbf{e}_1^s(\mathbf{r}) = 0, \quad \mathbf{j}_1(\mathbf{r}) = \mathbf{j}_1^{inc}(\mathbf{r}) + \mathbf{j}_1^s(\mathbf{r}) = \mathbf{J}_{1e}, \quad \mathbf{r} \in S_1 \\ \mathbf{e}_2(\mathbf{r}) = \mathbf{e}_2^{inc}(\mathbf{r}) + \mathbf{e}_2^s(\mathbf{r}) = \mathbf{n}_2 \times \mathbf{J}_{2m}, \quad \mathbf{j}_2(\mathbf{r}) = \mathbf{j}_2^{inc}(\mathbf{r}) + \mathbf{j}_2^s(\mathbf{r}) = \mathbf{J}_{2e}, \quad \mathbf{r} \in S_2 \end{cases}, \tag{3}$$

in which, $\mathbf{e} = \mathbf{n} \times \mathbf{E} \times \mathbf{n}$ and $\mathbf{j} = \mathbf{n} \times \mathbf{H}$ are the total tangential electric field and magnetic fields, respectively, and $\mathbf{e}^{inc}(\mathbf{r})$ and $\mathbf{j}^{inc}(\mathbf{r})$ are the incident wave's tangential electric field and magnetic fields, respectively. Further, we have:

$$\begin{aligned} \frac{\alpha}{\eta_0}\mathbf{e}_1^{inc}(\mathbf{r}) + \beta\mathbf{j}_1^{inc}(\mathbf{r}) =& -\alpha\mathbf{n}_1 \times L_0(\mathbf{J_{1e}}) \times \mathbf{n}_1 - \alpha\mathbf{n}_1 \times L_0(\mathbf{J}_{2e}) \times \mathbf{n}_1 + (\alpha/\eta_0)\mathbf{n}_1 \times \tilde{K}_0(\mathbf{J}_{2m}) \times \mathbf{n}_1 \\ & + (\beta/2)\mathbf{J_{1e}} - \beta\mathbf{n}_1 \times \tilde{K}_0(\mathbf{J_{1e}}) - (\beta/\eta_0)\mathbf{n}_1 \times L_0(\mathbf{J}_{2m}) - \beta\mathbf{n}_1 \times \tilde{K}_0(\mathbf{J}_{2e})\, \mathbf{r} \in S_1 \end{aligned} \tag{4a}$$

$$\begin{aligned} \frac{\alpha}{\eta_0}\mathbf{e}_2^{inc}(\mathbf{r}) + \beta\mathbf{j}_2^{inc}(\mathbf{r}) =& -\alpha\mathbf{n}_2 \times L_0(\mathbf{J_{1e}}) \times \mathbf{n}_2 - \alpha\mathbf{n}_2 \times L_0(\mathbf{J}_{2e}) \times \mathbf{n}_2 + \frac{\alpha}{2\eta_0}\mathbf{n}_2 \times \mathbf{J}_{2m} + \frac{\alpha}{\eta_0}\mathbf{n}_2 \times \tilde{K}_0(\mathbf{J}_{2m}) \times \mathbf{n}_2 \\ & - \beta\mathbf{n}_2 \times \tilde{K}_0(\mathbf{J_{1e}}) - (\beta/\eta_0)\mathbf{n}_2 \times L_0(\mathbf{J}_{2m}) + (\beta/2)\mathbf{J}_{2e} - \beta\mathbf{n}_2 \times \tilde{K}_0(\mathbf{J}_{2e})\, \mathbf{r} \in S_2 \end{aligned} \tag{4b}$$

with $\tilde{K}$ being the principle value integral, α and β the combination factors satisfying $0 \le \alpha, \beta \le 1$ and $\alpha + \beta = 1$. The electric and magnetic currents are expanded with RWG function: $\mathbf{J}_{1e} = \sum_{j=1}^{N_1} x_{1j}\mathbf{f}_{1j}(\mathbf{r})$, $\mathbf{J}_{2e} = \sum_{j=1}^{N_2} c_j\mathbf{f}_{2j}(\mathbf{r})$ and $\mathbf{J}_{2m} = \sum_{j=1}^{N_2} c_j\mathbf{f}_{2j}(\mathbf{r})$, in which $\mathbf{f}_{1j}$ and $\mathbf{f}_{2j}$ are the RWG basis functions [22] on S_1 and S_2, respectively. The total number of edges of S_1 is N_1, including the common edges [15] connected to S_1 and S_2, while the total number of edges of S_2 is N_2, excluding the common edges. In the frame of Galerkin method, choose test function $\mathbf{f}_{1i}$ and $\mathbf{f}_{2i}$ for Equation (4) to formulate the resultant matrix equation, simultaneously define the operator of two complex vectors as $\langle u, v\rangle_\Gamma = \int_\Gamma u \cdot v d\Gamma$. Equations (4a) and (4b) can be translated into:

$$\begin{bmatrix} Q_{11} \\ Q_{21} \end{bmatrix} \{x_1\} + \begin{bmatrix} Q_{12} & P_{12} \\ Q_{22} & P_{22} \end{bmatrix} \begin{bmatrix} c \\ d \end{bmatrix} = \begin{bmatrix} b_1 \\ b_2 \end{bmatrix}, \tag{5}$$

where

$$\begin{aligned} Q_{pp}(i,j) &= -\alpha \langle \mathbf{f}_{pi}, L_0(\mathbf{f}_{pj})\rangle_{T_{pi}} + (\beta/2)\langle \mathbf{f}_{pi}, \mathbf{f}_{pj}\rangle_{T_{pi}} - \beta\left\langle \mathbf{f}_{pi}, \mathbf{n}_{pi} \times \tilde{K}_0(\mathbf{f}_{pj})\right\rangle_{T_{pi}}, \\ & \quad i, j \in [1, N_p], \quad p = 1, 2, \end{aligned} \tag{6a}$$

$$\begin{aligned} Q_{pq}(i,j) &= -\alpha \langle \mathbf{f}_{pi}, L_0(\mathbf{f}_{qj})\rangle_{T_{pi}} - \beta\left\langle \mathbf{f}_{pi}, \mathbf{n}_{pi} \times \tilde{K}_0(\mathbf{f}_{qj})\right\rangle_{T_{pi}}, \\ & \quad i \in [1, N_p], \quad j \in [1, N_q], \quad \{p, q\} = \{1, 2\} \cup \{2, 1\}, \end{aligned} \tag{6b}$$

$$\begin{aligned} P_{12}(i,j) &= (\alpha/\eta_0)\left\langle \mathbf{f}_{1i}, \tilde{K}_0(\mathbf{f}_{2j})\right\rangle_{T_{1i}} - (\beta/\eta_0)\langle \mathbf{f}_{1i}, \mathbf{n}_{1i} \times L_0(\mathbf{f}_{2j})\rangle_{T_{1i}}, \\ & \quad i \in [1, N_1], \quad j \in [1, N_2], \end{aligned} \tag{6c}$$

$$\begin{aligned} P_{22}(i,j) &= \frac{\alpha}{2\eta_0}\langle \mathbf{f}_{2i} \times \mathbf{n}_{2i}, \mathbf{f}_{2j}\rangle_{T_{2i}} + (\alpha/\eta_0)\left\langle \mathbf{f}_{2i}, \tilde{K}_0(\mathbf{f}_{2j})\right\rangle_{T_{2i}} - (\beta/\eta_0)\langle \mathbf{f}_{2i}, \mathbf{n}_{2i} \times L_0(\mathbf{f}_{2j})\rangle_{T_{2i}}, \\ & \quad i, j \in [1, N_2], \end{aligned} \tag{6d}$$

$$\begin{aligned} b_p(i) &= (\alpha/\eta_0)\left\langle \mathbf{f}_{pi}, \mathbf{E}_p^{inc}\right\rangle_{T_{pi}} + \beta\left\langle \mathbf{f}_{pi}, \mathbf{n}_{2i} \times \mathbf{H}_p^{inc}\right\rangle_{T_{pi}}, \\ & \quad i \in [1, N_p], \quad p = 1, 2. \end{aligned} \tag{6e}$$

The resultant matrix Equation (5) has the size of $(N_1+N_2)\times(N_1+2N_2)$ which is not sufficient for the final electric and magnetic currents solution. Considering constructing other supplementary equations for Eq. (5), formulating equations based on JMCFIE in the interior domain is feasible, whereas this paper introduces single effective currents of the SIE method [14] rather than the original equivalent electric and magnetic currents of JMCFIE to represent the interior field. So the unknowns in the dielectric domain will be reduced by one half compared to JMCFIE. Therefore, this hybrid method SJMCFIE will be derived in the following.

In SJMCFIE method, the fields in the dielectric domain can be computed with effective current J_{2e}^{eff} on interior surface $S_d = S_2 + S_3$, with the expression of $\mathbf{E}_d = \eta_1 L_1(\mathbf{J}_{2e}^{eff}), \mathbf{H}_d = K_1(\mathbf{J}_{2e}^{eff})$. $\eta_1 = \sqrt{\mu/\varepsilon}$ being the wave impedance. Besides, in $L_1(\cdot)$, $K_1(\cdot)$ and $g(\mathbf{r}, \mathbf{r}')$, wave number is $k = w\sqrt{\mu\varepsilon}$. It is pointed out that the field represented by the effective currents satisfies the interior boundary condition on S_2:

$$\begin{cases} \mathbf{J}_{2e} = \mathbf{n}_2 \times \mathbf{H}_d = -\mathbf{J}_{2e}^{eff}/2 + \mathbf{n}_2 \times \tilde{K}_1(\mathbf{J}_{2e}^{eff}) \\ -\mathbf{J}_{2m} = \mathbf{n}_2 \times \mathbf{E}_d = \mathbf{n}_2 \times \eta_1 L_1(\mathbf{J}_{2e}^{eff}) \end{cases} \text{ on } S_2 \tag{7a}$$

and the boundary condition on the common surface S_3 of the dielectric and the conducting body:

$$-\alpha \mathbf{n}_3 \times L_1(\mathbf{J}_{2e}^{eff}) \times \mathbf{n}_3 - (\beta/2)\mathbf{J}_{2e}^{eff} - \beta \mathbf{n}_3 \times \tilde{K}_1(\mathbf{J}_{2e}^{eff}) = 0 \text{ on } S_3, \tag{7b}$$

where the effective current on S_3 has degenerated to surface equivalent current. Total effective currents on the dielectric object's interior surface can be expanded by RWG functions as $\mathbf{J}_{2e}^{eff}(r) = \sum_{i=1}^{N_2} x_{2i}\mathbf{f}_{2i} + \sum_{i=1}^{N_3} x_{3i}\mathbf{f}_{3i}$ with the number of unknown edges being $N_2 + N_3$. Among them, N_3 is the number of unknown edges on S_3 including the common edges. Referring to [14], the expansion coefficients can be approximated by the average values passing through the edges:

$$x_{pi} = (1/l_{pi}) \int_{l_{pi}} (\hat{l}_{pi} \times \mathbf{n}_{pi}) \cdot \mathbf{J}_{2e}^{eff}\, dl, \quad p = 2, 3. \tag{8}$$

Combining Equations (7a) and (8), expansion coefficients $\{c\}$ and $\{d\}$ in Eq. (5) can be expressed as:

$$\{c\} = [\tilde{P}_{22}]\{x_2\} + [\tilde{P}_{23}]\{x_3\}, \quad \{d\} = [\tilde{Q}_{22}]\{x_2\} + [\tilde{Q}_{23}]\{x_3\}, \quad \{0\} = [\tilde{Q}_{32}]\{x_2\} + [\tilde{Q}_{33}]\{x_3\}. \tag{9}$$

Here, $\{x_2\}$ and $\{x_3\}$ are the vectors of the expansion coefficients of single effective currents. In Eq. (9), submatrices' elements can be represented as:

$$\tilde{P}_{22}(i,j) = -(1/2)\delta_{ij} - \int_{l_{2i}} (\hat{l}_{2i}/l_{2i}) \cdot \tilde{K}_1(\mathbf{f}_{2j})dl, \quad i,j \in [1,N_2] \tag{10a}$$

$$\tilde{P}_{23}(i,j) = -\int_{l_{2i}} (\hat{l}_{2i}/l_{2i}) \cdot \tilde{K}_1(\mathbf{f}_{3j})dl, \quad i \in [1,N_2], \quad j \in [1,N_3] \tag{10b}$$

$$\tilde{Q}_{2q}(i,j) = \int_{l_{2i}} (\eta_1/l_{2i})\hat{l}_{2i} \cdot L_1(\mathbf{f}_{qj})dl, \quad i \in [1,N_2], \quad j \in [1,N_q], q = 2,3 \tag{10c}$$

$$\tilde{Q}_{32}(i,j) = -\alpha \langle \mathbf{f}_{3i}, L_1(\mathbf{f}_{2j}) \rangle_{T_{3i}} - \beta \left\langle \mathbf{f}_{3i}, \mathbf{n}_{3i} \times \tilde{K}_1(\mathbf{f}_{2j}) \right\rangle_{T_{3i}}, \quad i \in [1,N_3], \quad j \in [1,N_2] \tag{10d}$$

$$\tilde{Q}_{33}(i,j) = -\alpha \langle \mathbf{f}_{3i}, L_1(\mathbf{f}_{3j}) \rangle_{T_{3i}} - (\beta/2) \langle \mathbf{f}_{3i}, \mathbf{f}_{3j} \rangle_{T_{3i}} - \beta \left\langle \mathbf{f}_{3i}, \mathbf{n}_{3i} \times \tilde{K}_1(\mathbf{f}_{3j}) \right\rangle_{T_{3i}}, \quad i,j \in [1,N_3], \tag{10e}$$

where, if $i = j$, $\delta_{ij} = 1$; else if $i \neq j$, $\delta_{ij} = 0$. By substituting Eq. (9) into Eq. (5), new resultant matrix equation is obtained:

$$\begin{bmatrix} A_{11} & A_{12} & A_{13} \\ A_{21} & A_{22} & A_{23} \\ 0 & A_{32} & A_{33} \end{bmatrix} \begin{Bmatrix} x_1 \\ x_2 \\ x_3 \end{Bmatrix} = \begin{Bmatrix} b_1 \\ b_2 \\ 0 \end{Bmatrix}, \tag{11}$$

where

$$[A_{11}] = [Q_{11}], \quad [A_{12}] = [Q_{12}] \cdot [\tilde{P}_{22}] + [P_{12}] \cdot [\tilde{Q}_{22}], \quad [A_{13}] = [Q_{12}] \cdot [\tilde{P}_{23}] + [P_{12}] \cdot [\tilde{Q}_{23}],$$

$$[A_{21}] = [Q_{21}], \quad [A_{22}] = [Q_{22}] \cdot [\tilde{P}_{22}] + [P_{22}] \cdot [\tilde{Q}_{22}], \quad [A_{23}] = [Q_{22}] \cdot [\tilde{P}_{23}] + [P_{22}] \cdot [\tilde{Q}_{23}],$$

$$[A_{32}] = [\tilde{Q}_{32}], \quad [A_{33}] = [\tilde{Q}_{33}].$$

Due to adopting SIE, Equation (11) has the number of unknowns $N_1 + N_2 + N_3$ less than one of $N_1 + 2N_2 + N_3$ based on JMCFIE. We substitute $x_3 = -A_{33}^{-1}A_{32}x_2$ into Eq. (11), and a new matrix equation is derived:

$$\begin{bmatrix} A_{11}(A_{12} - A_{13}A_{33}^{-1}A_{32}) \\ A_{21}(A_{22} - A_{23}A_{33}^{-1}A_{32}) \end{bmatrix} \begin{Bmatrix} x_1 \\ x_2 \end{Bmatrix} = \begin{Bmatrix} b_1 \\ b_2 \end{Bmatrix}, \tag{12}$$

among which the number of unknowns $N_1 + N_2$ is less than $N_1 + N_2 + N_3$ in Eq. (11). $A_{13}A_{33}^{-1}A_{32}$ represents indirectly mutual interaction between the dielectric exterior surface S_2 and the conductor's exterior surface S_1. A_{32} denotes the interaction between S_2 and the common surface S_3. A_{33}^{-1} denotes the self-interaction of S_3. A_{31} denotes the interaction between S_1 and S_3. In a word, the indirectly mutual interaction's process is $S_2 \rightarrow S_3 \rightarrow S_1$.

Similarly, $A_{23}A_{33}^{-1}A_{32}$ indirectly represents self-interaction of the dielectric exterior surface S_2, which has the process of $S_2 \rightarrow S_3 \rightarrow S_2$.

When total number of unknowns is relatively low, directly solving Eq. (12) is enough; however, with number of unknowns getting higher, iterative solvers, such as Bi-Conjugate Gradients Stabilized Approach (BiCGSTAB) and Generalized Minimum Residual (GMRES) method [23], can effectively reduce the computation complexity. It is worth to note that during per iteration, A_{33}^{-1} concerns the matrix inversion, and in practice, we may translate $A_{33}^{-1}a = b$ into $A_{33}^{b} = a$, which can also be solved to achieve MVM $A_{33}^{-1}a$ by the iteration method. When N_3 gets large, solving iteratively $A_{33}^{b} = a$ costs more time, so Equation (11) is a better choice. Actually, SIE not only reduces the number of unknowns, but also improves the matrix condition number deduced from EFIE or combined field integral equation. As we know, matrix equation's convergence performance is potentially determined by matrix condition number. Noticeably, magnetic field integral operator belongs to the second-kind Fredholm operator or compact operator, whereas electric field integral operator belongs to the first-kind Fredholm operator or non-compact operator [20]. Compact operator makes the matrix condition number better than non-compact operator because the former is well conditioned. JMCFIE includes non-compact operator or electric field integral operator in the dielectric domain that will worsen its matrix condition number, whereas SJMCFIE includes two-fold operators in the dielectric domain such as $L_0 \cdot \tilde{K}_1$, $\tilde{K}_0 \cdot L_1$, $L_0 \cdot L_1$. The multiplication of compact and non-compact operators is still a compact operator [20, 21], so the two former ones are compact operators. And the third term is the multiplication of two non-compact operators and is also a compact operator [13]. As a result, SJMCFIE improves matrix condition number in the dielectric domain. Iteration convergence will be improved and iteration steps reduced if adopting iteration methods for solving the resultant matrix equation. This conclusion has been numerically validated by Yeung in [14] when solving scattering from the pure dielectric object. Wang et al. attempt to incorporate SIE with EFIE, and as a result, the process of translating non-compact operator is similar to that in SJMCFIE. However, the conducting part is still based on EFIE, and obviously, this makes iteration convergence slow compared to combined field integral equation in SJMCFIE. Finally, the formulating process of resultant matrix equation in JMCFIE will cost more time than that in SJMCFIE, which will be verified in Section 3.

2.2. Formulation of SJMCFIE-MLFMA

When adopting iteration solvers to solving resultant matrix equation of SJMCFIE, most of MVMs per iteration will increase total computation complexity. For mitigating this problem, this paper introduces MLFMA to SJMCFIE. In detail, for the resultant matrix Equation (12), according to the interaction between basis functions, the impedances of each submatrix can be divided into near-region parts and well-separated parts, in which the former can only be directly computed by the method of moments (MOM), and the latter can be approximated by MLFMA. In essence, MLFMA utilizes tree-grouping concept. Detailed process is: initially define a box enclosing the whole composite objects, which is marked as the zero level, then divide this box into eight subboxes to form the first level, and after that, divide these subboxes into finer subboxes. Recursively, the finest level is denoted as L_f whose box's length D_f is about 0.3λ, in which λ is the wave length in the free space. These boxes are always called groups. The above grouping process generates an oct-tree. Remember that only non-empty box on each level is marked as an exclusive index, and computation process is based on these non-empty boxes/groups. In the detailed implementation, MLFMA includes three important processes: aggregation, translation and disaggregation, in which the translation process is performed level by level from the finest to the coarsest, and at some level, only concerns the well-separated groups that are non-overlapping or adjacent, but their parents' groups are adjacent [17]. In what follows, some brief formulations about how to incorporate SJMCFIE with MLFMA are given. Some more detailed descriptions about MLFMA can be found in [17].

At some level, utilizing the addition theorem [17], Green's function and its Gradient can be expanded with the form of

$$e^{-jk_0r_{ij}}/r_{ij} = -j(k_0/4\pi)\int_{S_E} d^2\hat{k}e^{-j\mathbf{k}\cdot(\mathbf{r}_{im}-\mathbf{r}_{jm'})}T_0(k,\hat{r}_{mm'}) \tag{13a}$$

$$\nabla(e^{-jk_0r_{ij}}/r_{ij}) = -[k_0^2/(4\pi)]\int_{S_E} \hat{k}d^2\hat{k}e^{-j\mathbf{k}\cdot(\mathbf{r}_{im}-\mathbf{r}_{jm'})}T_0(k,\hat{r}_{mm'}) \tag{13b}$$

where

$$T_0(k,\hat{r}_{mm'}) = \sum\nolimits_{l=0}^{L}(-j)^l(2l+1)h_l^{(2)}(k_0r_{mm'})P_l(\hat{k}\cdot\hat{r}_{mm'}).$$

Here, $\mathbf{r}_i$ is a field point locating in m-th group with the center $\mathbf{r}_m$, and $\mathbf{r}_j$ is a source point locating in m'-th group with the center $\mathbf{r}_{m'}$, satisfying $\mathbf{r}_{im} = \mathbf{r}_i - \mathbf{r}_m$, $\mathbf{r}_{jm'} = \mathbf{r}_j - \mathbf{r}_{m'}$ and $\mathbf{r}_{mm'} = \mathbf{r}_m - \mathbf{r}_{m'}$. S_E stands for the Ewald spherical surface [24], and $\hat{k}$ is the unit angular direction, $k = k_0\hat{k}$. $h_l^{(2)}$ is the Hankel function of the 2^{nd} kind. P_l is the Legendre polynomial. L is the number of modes referring to [16]. Substituting Eq. (13) into Eq. (6), the well-separated group's impedances can be approximated as

$$\begin{aligned}
&Q_{pq}(i,j) = \int_{S_E} d^2\hat{k}U_{im}^{Q_{pp}}\cdot T_0(k,\hat{r}_{mm'})V_{jm'}^{Q_{qq}}, \quad p,\, q = 1,2\\
&P_{pq}(i,j) = \int_{S_E} d^2\hat{k}U_{im}^{P_{pp}}\cdot T_0(k,\hat{r}_{mm'})V_{jm'}^{P_{qq}}, \quad p = 1,2;\ q = 2\\
&U_{im}^{Q_{pp}} = [k_0^2/(16\pi^2)][\alpha\int_{T_{pi}} dse^{-j\mathbf{k}\cdot\mathbf{r}_{im}}f_{pi}\cdot(\bar{\bar{I}}-\hat{k}\hat{k}) + \beta\hat{k}\times\int_{T_{pi}} dse^{-j\mathbf{k}\cdot\mathbf{r}_{im}}(\mathbf{n}_{pi}\times\mathbf{f}_{pi})], \quad p = 1,2\\
&U_{im}^{P_{pp}} = [k_0^2/(16\pi^2\eta_0)][\alpha\int_{T_{pi}} ds(\hat{k}\times\mathbf{f}_{pi})e^{-j\mathbf{k}\cdot\mathbf{r}_{im}} + \beta\int_{T_{pi}} dse^{-jk\cdot r_{im}}(\mathbf{f}_{pi}\times\mathbf{n}_{pi})\cdot(\bar{\bar{I}}-\hat{k}\hat{k})], \quad p = 1,2\\
&V_{jm'}^{Q_{qq}} = V_{jm'}^{P_{qq}} = \int_{T_{qj}} ds'e^{j\mathbf{k}\cdot\mathbf{r}_{jm'}}\mathbf{f}_{qj}\cdot(\bar{\bar{I}}-\hat{k}\hat{k}), \quad q = 1,2
\end{aligned} \tag{14}$$

However, for Equation (9), wave number, wave impedance and Green's function should be replaced with k, η_1 and g with respect to ε, μ in the dielectric region. So in Equation (9), the well-separated group's impedances can be approximated as

$$\begin{aligned}
&\tilde{P}_{2q}(i,j) = \int_{S_E} d^2\hat{k}U_{im}^{\tilde{P}_{22}}\cdot T_1(k_1,\hat{r}_{mm'})V_{jm'}^{\tilde{P}_{qq}}, \quad q = 2,3\\
&\tilde{Q}_{2q}(i,j) = \int_{S_E} d^2\hat{k}U_{im}^{\tilde{Q}_{22}}\cdot T_1(k_1,\hat{r}_{mm'})V_{jm'}^{\tilde{Q}_{qq}}, \quad q = 2,3\\
&\tilde{Q}_{3q}(i,j) = \int_{S_E} d^2\hat{k}U_{im}^{\tilde{Q}_{33}}\cdot T_1(k_1,\hat{r}_{mm'})V_{jm'}^{\tilde{Q}_{qq}}, \quad q = 2,3\\
&U_{im}^{\tilde{P}_{22}} = [k^2/(l_{2i}16\pi^2)]\int_{l_{2i}} dl(\hat{l}_{2i}\times\hat{k})e^{-j\mathbf{k}_1\cdot\mathbf{r}_{im}},\\
&U_{im}^{\tilde{Q}_{22}} = -[(\eta_1k^2)/(l_{2i}16\pi^2)]\int_{l_{2i}} dle^{-j\mathbf{k}_1\cdot\mathbf{r}_{im}}\widehat{l}_{2i}\cdot(\bar{\bar{I}}-\hat{k}\hat{k}),\\
&U_{im}^{\tilde{Q}_{33}} = [k^2/(16\pi^2)]\left[\alpha\int_{T_{pi}} dse^{-j\mathbf{k}_1\cdot\mathbf{r}_{im}}\mathbf{f}_{3i}\cdot(\bar{\bar{I}}-\hat{k}\hat{k}) + \beta\hat{k}\times\int_{T_{pi}} dse^{-j\mathbf{k}_1\cdot\mathbf{r}_{im}}(\mathbf{n}_{3i}\times\mathbf{f}_{3i})\right],\\
&V_{jm'}^{\tilde{P}_{qq}} = V_{jm'}^{\tilde{Q}_{qq}} = \int_{T_{qj}} ds'e^{j\mathbf{k}_1\cdot\mathbf{r}_{jm'}}\mathbf{f}_{qj}\cdot(\bar{\bar{I}}-\hat{k}\hat{k}), \quad q = 2,3
\end{aligned} \tag{15}$$

in which, $\mathbf{k}_1 = k\hat{k}$, and U_{im}, $V_{jm'}$ and T_0/T_1 are the receiving pattern, radiation pattern and translation pattern respectively. Substituting Eqs. (14) and (15) into Eqs. (5) and (9), we have:

$$\begin{aligned}
Q_{pq} &= Q_{pq}^{near} + \sum_{l=2}^{L_f} U_{Q_{pp}}^{(l)} T_0^{(l)} V_{Q_{qq}}^{(l)}, \quad p,q = 1,2 \\
P_{pq} &= P_{pq}^{near} + \sum_{l=2}^{L_f} U_{P_{pp}}^{(l)} T_0^{(l)} V_{P_{qq}}^{(l)}, \quad p,q = 1,2 \\
\tilde{P}_{2q} &= \tilde{P}_{2q}^{near} + \sum_{l=2}^{L_f} U_{\tilde{P}_{22}}^{(l)} T_1^{(l)} V_{\tilde{P}_{qq}}^{(l)}, \quad q = 2,3 \\
\tilde{Q}_{2q} &= \tilde{Q}_{2q}^{near} + \sum_{l=2}^{L_f} U_{\tilde{Q}_{22}}^{(l)} T_1^{(l)} V_{\tilde{Q}_{qq}}^{(l)}, \quad q = 2,3 \\
\tilde{Q}_{3q} &= \tilde{Q}_{3q}^{near} + \sum_{l=2}^{L_f} U_{\tilde{Q}_{33}}^{(l)} T_1^{(l)} V_{\tilde{Q}_{qq}}^{(l)}, \quad q = 2,3
\end{aligned} \tag{16}$$

Here, the L_fth level is the finest level, and L_f is the number of total levels. $U^{(l)}$, $V^{(l)}$ and $T_0^{(l)}/T_1^{(l)}$ are the disaggregation, aggregation and translation matrices at the l-th level, respectively, in which $U^{(l)}$ and $V^{(l)}$ are composed of U_{im} and $V_{jm'}$ in Eqs. (14) and (15). The translation matrices at each level, and aggregation and disaggregation matrices at the finest level may be precomputed and stored, which can utilize the symmetry of unit angular directions $\widehat{k}$ to optimize storage requirement. As we know, MLFMA is used to accelerate MVMs per iteration and usually includes two sweeps: during the first sweep, the main implementation concerns the aggregation and translation processes. In detail, different from computing the aggregation matrices at the finest level, at the other levels the aggregation ones are indirectly computed by interpolation level-by-level from the $(L_f - 1)$-th level to the second level. Simultaneously, the translation process about the well-separated groups is also done with the above aggregation process. During the second sweep, the incoming waves composed of aggregation and translation matrices' elements with respect to some receiving group are computed level-by-level from the second level to the finest level by shifting and anterpolation [17]. After the above two sweeps, multiplying incoming waves by disaggregation matrices' elements realizes the reduction of MVMs' complexity in the resultant matrix Equation (12).

If adopting iteration method to solving Equation (11), the cost of one MVM in SJMCFIE is $(N_1 + N_2 + N_3)^2$, and for JMCFIE, the cost of one MVM is $(N_1 + N_2)^2 + (N_1 + N_2)N_2$ on the exterior surfaces of S_1 and S_2, and is $(N_2 + N_3)^2 + (N_2 + N_3)N_2$ on S_3 and interior surface of S_2, so the whole cost of one MVM in JMCFIE is $(N_1 + N_2)^2 + (N_2 + N_3)^2 + (N_1 + 2N_2 + N_3)N_2$. Obviously, SJMCFIE has lower cost of one MVM than JMCFIE. Furthermore, because the condition number of SJMCFIE is better than that of JMCFIE as shown in Subsection 2.1, SJMCFIE has faster convergence property than JMCFIE. When combining MLFMA with SJMCFIE, redundant computations concerning sub-matrices' MVMs will emerge and can be reduced. In detail, $[Q_{11}]\{x_1\}$ and $[Q_{21}]\{x_1\}$ have the same aggregation terms for Equation (11). This property is also reflected in $[\tilde{P}_{22}]\{x_2\}$, $[\tilde{Q}_{22}]\{x_2\}$ and $[\tilde{Q}_{32}]\{x_2\}$, as well as $[\tilde{P}_{23}]\{x_3\}$, $[\tilde{Q}_{23}]\{x_3\}$ and $[\tilde{Q}_{33}]\{x_3\}$. After setting $\{y\} = [\tilde{P}_{22}]\{x_2\}$, $\{y'\} = [\tilde{Q}_{22}]\{x_2\}$, $\{z\} = [\tilde{P}_{23}]\{x_3\}$, $\{z'\} = [\tilde{Q}_{23}]\{x_3\}$, the property of having the same aggregation terms is also reflected in $[Q_{12}]\{y\}$ and $[Q_{22}]\{y\}$, $[P_{12}]\{y'\}$ and $[P_{22}]\{y'\}$, $[Q_{12}]\{z\}$ and $[Q_{22}]\{z\}$, $[P_{12}]\{z'\}$ and $[P_{22}]\{z'\}$, respectively. So the cost of one MVM is $O((N_1 + N_2)\log(N_1 + N_2))$ on the exterior surfaces of S_1 and S_2 and on the exterior surfaces of S_1 and S_2 on composite objects' exterior surface, and the cost of one MVM reaches $O((N_2 + N_3)\log(N_2 + N_3))$ on S_3 and interior surface of S_2, so SJMCFIE-MLFMA has the computation complexity of $O((N_1 + N_2)\log(N_1 + N_2) + (N_2 + N_3)\log(N_2 + N_3))$. Similarly, for JMCFIE-MLFMA, the cost of one MVM is $O((N_1 + 2N_2)\log(N_1 + 2N_2))$ on the exterior surfaces of S_1 and S_2 and is $O((2N_2 + N_3)\log(2N_2 + N_3))$ on S_3 and interior surface of S_2, so it has the computation complexity of $O((N_1 + 2N_2)\log(N_1 + 2N_2) + (2N_2 + N_3)\log(2N_2 + N_3))$. Obviously, computation complexity of JMCFIE-MLFMA is more than that of the proposed method, which will be verified in the next section.

As we see, hybrid method SJMCFIE-MLFMA is an extension of SIE-MLFMA in [15] due to (i) adopting JMCFIE rather than EFIE in SIE-MLFMA; (ii) Equation (12) explicitly reflecting coupling mechanism of the composite model; (iii) better condition number of resultant matrix. So the new hybrid method makes total computation more efficient than SIE-MLFMA.

3. NUMERICAL RESULTS AND DISCUSSION

3.1. A Composite Sphere

For verifying the validation of SJMCFIE-MLFMA, see a composite sphere composed of a perfecting conducting (PEC) hemisphere and a dielectric hemisphere with the relative permittivity $\varepsilon_r = 3.0$. The radius of this composite sphere is $6.0\lambda_0$ with λ_0 the wavelength in free space. We have a total of 102625 triangular patches with a length less than $0.09\lambda_0$ to model this composite sphere including 153938 unknowns if adopting SJMCFIE-MLFMA or SIE-MLFMA while 216175 unknowns have to be calculated if adopting JMCFIE-MLFMA.

For comparing the precision of these methods, define the root mean square error (RMSE) of

$$\mathrm{RMSE} = \sqrt{\frac{1}{N}\sum_{m=1}^{N} |RCS^{Calculated} - RCS^{JMCFIE}|^2}, \tag{17}$$

where N is the number of unknowns of the recorded azimuth.

Figure 2 shows the bistatic RCS of the composite sphere by SJMCFIE-MLFMA, SIE-MLFMA in [15] and JMCFIE-MLFMA. The parameters with respect to MLFMA have $D_f = 0.2\lambda_0$, $L_f = 6$, and $L = 11$ satisfying $L = k_0 D_f + 5\ln(\pi + k_0 D_f)$ in outer domain of composite objects; $D_f = 0.2\lambda$ with λ being the wavelength in dielectric part, $L_f = 7$, and $L = 11$ satisfying $L = kD_f + 5\ln(\pi + kD_f)$ in the dielectric part. The computing platform is AMD processor of 2.3 GHz with 64 kernels and 64 GB RAM adopting Microsoft Visual C++ programming language. BICGSTAB is chosen as the iteration solver. Set relative error of unknown currents to be 10^{-5}. Fig. 2 shows that the results by SJMCFIE-MLFMA and SIE-MLFMA are in good agreement with that by JMCFIE-MLFMA.

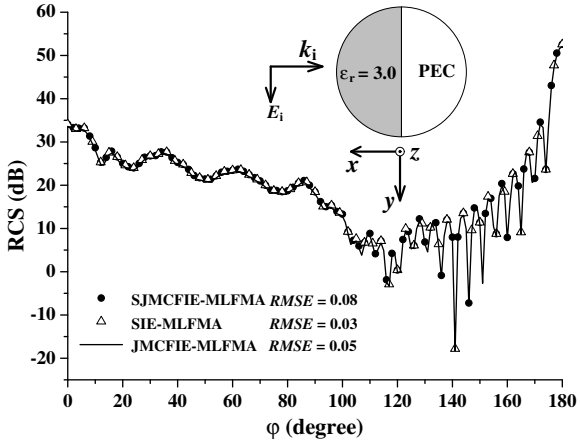

Figure 2. The bistatic RCS curves of a composite sphere by three kinds of methods.

Also, Table 1 gives a detailed comparison of these three methods. JMCFIE-MLFMA costs more time in matrix filling process than SJMCFIE-MLFMA and SIE-MLFMA, because in the dielectric's interior surface, the equation's form of JMCFIE-MLFMA is similar to Equation (4). As a result, both of the electric and magnetic currents concern two integral operators $L_1(\cdot)$ and $K_1(\cdot)$ compared to the single effective currents concerning $L_1(\cdot)$ and $K_1(\cdot)$. SIE-MLFMA and SJMCFIE-MLFMA have less computation time per iteration than JMCFIE-MLFMA, which verifies the result in Subsection 2.2. SIE-MLFMA is more efficient than SJMCFIE-MLFMA for which in conducting part the former only

Table 1. Comparison of SIE-MLFMA, JMCFIE-MLFMA and SJMCFIE-MLFMA.

	Matrix-filling time (s)	Storage requirement (GB)	Computation time per iteration (s)	Iteration steps	Total computation time (s)
SIE-MLFMA	203	5.862	5.3	224	1390.2
JMCFIE-MLFMA	369.8	8.152	7.8	120	1305.8
SJMCFIE-MLFMA	256	5.878	6.365	48	561.52

adopts EFIE, and the latter adopts CFIE. Due to better condition number of SJMCFIE, it needs the least iteration steps and total computation time.

3.2. A Bullet-shaped Composite Model

Another example is a bullet-shaped composite model illustrated in Fig. 3 including its geometric parameters. This model is composed of a conducting cylinder and coated head. The coated structure has the elliptical cross section with elliptical radii being a, b for the inner conductor and a_1, b_1 for the outer coated layer.

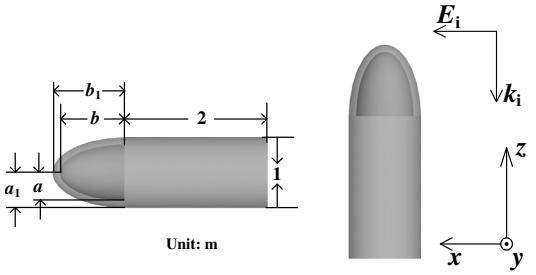

Figure 3. The bullet-shaped composite model composed of the conducting cylinder and coated.

The working frequency is 2 GHz, and the incident wave illuminates the composite model with the incident angle $\theta = 0^\circ$ and the polarization direction along x-axis. Computing platform and iteration solver are similar to that in the above example. Set the length of discretized patches to less than $0.09\lambda_0$, $0.05\lambda_0$, $0.03\lambda_0$ for the coated layer's permittivity $\varepsilon_r = 3.0$, 5.0, 8.0, respectively. Fig. 4(a) gives the bistatic RCS curves with different coated materials, while the coated structure has $a = 0.4$ m, $b = 0.9$ m, and the thickness has $t = (a_1 - a) = (b_1 - b) = 0.1$ m. The parameters with respect to MLFMA satisfy $D_f = 0.2\lambda_0$ and $L_f = 7$, $L = 11$ in outer domain of composite objects. In the coated head's domain, set λ to be the wavelength in dielectric part, and if relative permittivity has $\varepsilon_r = 3.0$, the coated domain has $D_f = 0.2\lambda$, $L_f = 6$, $L = 11$; if relative permittivity has $\varepsilon_r = 5.0$, the coated domain has $D_f = 0.24\lambda$, $L_f = 6$, $L = 12$; if relative permittivity has $\varepsilon_r = 8.0$, the coated domain has $D_f = 0.2\lambda$, $L_f = 7$, $L = 11$. The bistatic RCS curves are located on the x-z plane. Fig. 4(a) indicates that in total, with the coated material's relative permittivity getting small, backscattering will decrease.

Figure 4(b) gives the bistatic RCS curves of the bullet-shaped composite model with different coated layer thicknesses t. The working frequency and cylinder part's geometric parameter are similar to that in Fig. 3. The coated material has the relative permittivity $\varepsilon_r = 5.0$, and coated layer has the maximum patch's length of $0.05\lambda_0$. Set $a_1 = 0.5$ m, $b_1 = 1$ m. The parameters with respect to MLFMA satisfy $D_f = 0.2\lambda_0$ and $L_f = 7$, $L = 11$ in outer domain of composite objects, and $D_f = 0.24\lambda$ with λ being the wavelength in dielectric part, $L_f = 6$, $L = 12$ in the coated material's domain. The bistatic RCS curves are located on the x-z plane. As we see, when $t = 0$, the composite model degenerates a PEC object, and backscattering decreases. With the increase of thickness t, $t = 0.1$ m, backscattering will increase; however, during the directions ranging from 20° to 40°, the scattering curve has a deep drop. When $t = 0.2$ m, backscattering in directions ranging from 20° to 80° will increase compared to

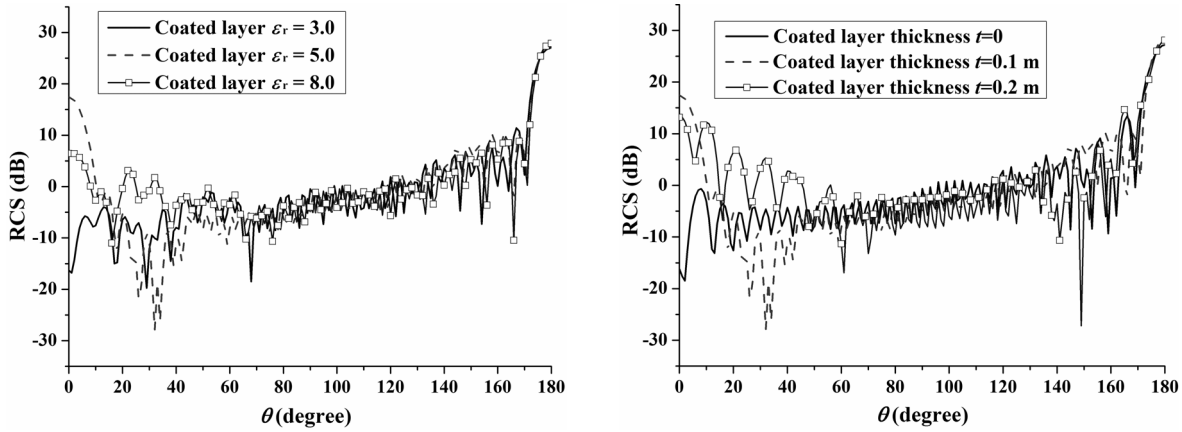

Figure 4. The bistatic RCS curves of the bullet-shaped composite model with different coated layer material and thickness.

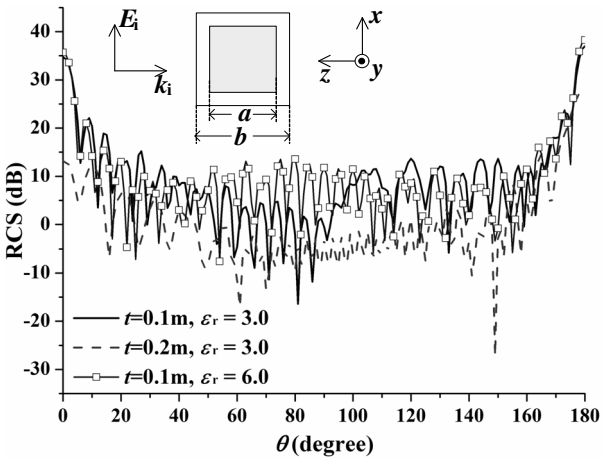

Figure 5. The bistatic RCS curves of the coated cube with different coated layer's thickness and relative permittivity.

that of $t = 0$ and $t = 0.1$ m. This example indicates that under the special condition, the coated layer thickness increases, and the backward RCS of the bullet-shaped composite model will increase.

3.3. The Coated Object

Another typical composite model is the coated cube. It can also be computed by SJMCFIE-MLFMA, except that S_1 does not exist. Equation (11) can be reduced to the form of

$$\begin{bmatrix} A_{22} & A_{23} \\ A_{32} & A_{33} \end{bmatrix} \begin{Bmatrix} x_2 \\ x_3 \end{Bmatrix} = \begin{Bmatrix} b_2 \\ 0 \end{Bmatrix}, \tag{18}$$

The inner conducting cube's length a equals 1.5 m, and the coated layer's thickness is $t = (b-a)/2$. Set the working frequency as 2 GHz, the incident direction as $\theta = 0^\circ$, $\varphi = 0^\circ$, and scattering curves located on the x-z plane.

Figure 5 gives the comparison of different coated layer's thicknesses and relative permittivities. Suppose that the maximum patch length is $0.09\lambda_0$ with coated material's permittivity $\varepsilon_r = 3.0$. The maximum patch length is $0.04\lambda_0$ with coated material's permittivity $\varepsilon_r = 6.0$. When $t = 0.1$ m, the parameters with respect to MLFMA are $D_f = 0.2\lambda_0$, $L_f = 6$ and $L = 11$ in the outer domain of the

coated object, are $D_f = 0.2\lambda$, $L_f = 7$ and $L = 11$ in the interior domain of the coated material with $\varepsilon_r = 3.0$, and are $D_f = 0.22\lambda$, $L_f = 7$ and $L = 11$ in the interior domain of the coated material with $\varepsilon_r = 6.0$. When $t = 0.2$ m, the parameters with respect to MLFMA are $D_f = 0.2\lambda_0$, $L_f = 6$ and $L = 11$ in the outer domain of the coated object, are $D_f = 0.2\lambda$, $L_f = 7$ and $L = 11$ in the interior domain of the coated material with $\varepsilon_r = 3.0$, and are $D_f = 0.2\lambda$, $L_f = 8$ and $L = 11$ in the interior domain of the coated material with $\varepsilon_r = 6.0$. As depicted in Fig. 5, under the condition of the same relative permittivity, scattering in almost all the directions will decrease with the thickness increasing, and under the condition of the same thickness, backscattering in directions ranging from 50° to 90° will decrease with the relative permittivity decreasing. This example illuminates that SJMCFIE-MLFMA can be applied in designing the coated layer to change the distribution of scattering energy. Simultaneously, due to this hybrid method's high efficiency and accuracy, it can be incorporated with fast frequency or angular sweeping techniques to reduce the complexity in computing frequency or angular response.

4. CONCLUSION

This paper proposes a highly efficient hybrid method of SJMCFIE-MLFMA by combining SIE and MLFMA based on JMCFIE for computing composite conductor and dielectric objects. More details about formulating SJMCFIE-MLFMA are shown including the formulation of SJMCFIE and how to combine MLFMA with SJMCFIE. The final resultant matrix equation has fewer unknowns than that by JMCFIE, and this hybrid method based on JMCFIE is an extension of SIE-MLFMA based EFIE in the proposed reference, therefore has higher efficiency than SIE-MLFMA. Examples verify the accuracy and efficiency of this new hybrid method in computing composite models. Due to high efficiency and accuracy in computing composite conductor and dielectric objects, this hybrid method can be used in designing a local coated structure to effectively reduce backscattering. Besides, SJMCFIE-MLFMA also can be used in analyzing scattering from the complete coated model. This paper indicates that the scheme of combining SIE with MLFMA based on JMCFIE is feasible in analyzing scattering from the composite model composed of a single conductor and a single dielectric body. In the following, we focus on extending SJMCFIE-MLFMA to compute more complicated composite models composed of multi-objects with different dielectric materials.

ACKNOWLEDGMENT

The authors thank the National Natural Science Foundation of China (Grant No. 61372033).

REFERENCES

1. Harrington, R. F., *Field Computation by Moment Methods*, Oxford University Press, Oxford, England, 1996.
2. Peterson, A. and R. Mittra, "Convergence of the conjugate gradient method when applied to matrix equaitions representing electromagnetic scattering problems," *IEEE Trans. Antennas Propag.*, Vol. 34, No. 12, 1447–1454, 1986.
3. Volakis, J. L. and K. Sertel, *Integral Equation Methods for Electromagnetics*, SciTech Publishing, Raleigh, NC, USA, 2012.
4. Ylä-Oijala, P. and M. Taskinen, "Application of combined field integral equation for electromagnetic scattering by dielectric and composite objects," *IEEE Trans. Antennas Propag.*, Vol. 53, No. 3, 1168–1173, 2005.
5. Ewe, W. B., L. W. Li, and M. S. Leong, "Fast solution of mixed dielectric/conducting scattering problem using volumesurface adaptive integral method," *IEEE Trans. Antennas Propag.*, Vol. 46, No. 11, 3071–3077, 2004.
6. Eibert, T. F., "Some scattering results computed by surface-integral-equation and hybrid finite-element-boundary-integral techniques, accelerated by the multilevel fast multipole method," *IEEE Antennas Propag. Mag.*, Vol. 49, No. 2, 61–69, 2007.

7. Ylä-Oijala, P., M. Taskinen, and S. Järvenpää, "Analysis of surface integral equations in electromagnetic scattering and radiation problems," *Engineering Analysis with Boundary Elements*, Vol. 32, 196209, 2008.
8. Donepudi, K. C., L. M. Jin, and W. C. Chew, "A higher order multilevel fast multipole algorithm for scattering from mixed conducting/dielectric bodies," *IEEE Trans. Antennas Propag.*, Vol. 2, No. 11, 2814–2821, 2002.
9. Ylä-Oijala, P., M. Taskinen, and J. Sarvas, "Surface integral equation method for general composite metallic and dielectric structures with junctions," *Progress In Electromagnetics Research*, Vol. 52, 81–108, 2005.
10. Ubeda, E., J. M. Tamayo, and J. M. Rius, "Taylor-orthogonal basis functions for the discretization in method of moments of second kind integral equations in the scattering analysis of perfectly conducting or dielectric objects," *Progress In Electromagnetics Research*, Vol. 119, 85–105, 2011.
11. Ergül Ö and L. Gürel, "Fast and accurate analysis of large-scale composite structures with the parallel multilevel fast multipole algorithm," *J. Opt. Soc. Amer. A*, Vol. 30, No. 30, 509–517, 2013.
12. Lu, C. C. and Z. Y. Zeng, "Scattering and radiation modeling using hybrid integral approach and mixed mesh element discretization," *PIERS Online*, Vol. 1, 70–73, 2005.
13. Ylä-Oijala, P. and M. Taskinen, "Well-conditioned Müller formulation for electromagnetic scattering by dielectric objects," *IEEE Trans. Antennas Propag.*, Vol. 53, No. 10, 3316–3323, 2005.
14. Yeung, M. S., "Single integral equation for electromagnetic scattering by three-dimensional homogeneous dielectric objects," *IEEE Trans. Antennas Propag.*, Vol. 47, No. 10, 1615–1622, 1999.
15. Wang, P., M. Y. Xia, and L. Z. Zhou, "Analysis of scattering by composite conducting and dielectric bodies using the single integral equation method and multilevel fast multipole algorithm," *Microw. and Opt. Tech. Lett.*, Vol. 48, No. 6, 1154–1156, 2006.
16. Song, J. M., C. C. Lu, and W. C. Chew, "Multilevel fast multipole algorithm for electromagnetic scattering by large complex objects," *IEEE Trans. Antennas Propag.*, Vol. 45, No. 10, 1488–1493, 1997.
17. Chew, W. C., J. M. Jin, E. Michielssen, and J. M. Song, *Fast and Efficient Algorithms in Computational Electromagnetics*, Artech House, Boston, MA, 2001.
18. Greengard, L. and V. Rokhlin, "A fast algorithm for particle simulations," *J. Comput. Phys.*, Vol. 73, 325–348, 1987.
19. Yan, S., J.-M. Jin, and Z. P. Nie, "Improving the accuracy of the second-kind Fredholm integral equations by using the Buffa-Christiansen functions," *IEEE Trans. Antennas Propag.*, Vol. 59, No. 4, 1299–1310, 2011.
20. Yan, S., J.-M. Jin, and Z. P. Nie, "A comparative study of Calderon preconditioners for PMCHWT equations," *IEEE Trans. Antennas Propag.*, Vol. 58, No. 7, 2375–2383, 2010.
21. Budko, N. V. and A. B. Samokhin, "Spectrum of the volume integral operator of electromagnetic scattering," *SIAM J. Sci. Comput.*, Vol. 28, No. 2, 682–700, 2005.
22. Rao, S. M., D. R. Wilton, and A. W. Glisson, "Electromagnetic scattering by surfaces of arbitrary shape," *IEEE Trans. Antennas Propag.*, Vol. 30, No. 3, 409–418, 1982.
23. Saad, Y., *Iterative Methods for Sparse Linear Systems*, PWS Publishing Company, Boston, 1996.
24. Cui, T. J., W. C. Chew, G. Chen, and J. M. Song, "Efficient MLFMA, RPFMA, and FAFFA algorithms for EM scattering by very large structures," *IEEE Trans. Antennas Propag.*, Vol. 52, No. 3, 759–770, 2004.